ACSNANO
www.acsnano.org
ARTICLE

$CsPb_xMn_{1-x}Cl_3$ Perovskite Quantum Dots with High Mn Substitution Ratio

Huiwen Liu,[†] Zhennan Wu,[†] Jieren Shao,[†] Dong Yao,[†] Hang Gao,[†] Yi Liu,[†] Weili Yu,[‡] Hao Zhang,*[,†] and Bai Yang[†]

[†]State Key Laboratory of Supramolecular Structure and Materials, College of Chemistry, Jilin University, Changchun 130012, People's Republic of China

[‡]The China–US Joint Laboratory, Changchun Institute of Optics, Fine Mechanics and Physics, Chinese Academy of Science, Changchun, 130033, People's Republic of China

Supporting Information

ABSTRACT: **$CsPbX_3$ (X = Cl, Br, I) perovskite quantum dots (QDs) are potential emitting materials for illumination and display applications, but toxic Pb is not environment- and user-friendly. In this work, we demonstrate the partial replacement of Pb with Mn through phosphine-free hot-injection preparation of $CsPb_xMn_{1-x}Cl_3$ QDs in colloidal solution. The Mn substitution ratio is up to 46%, and the as-prepared QDs maintain the tetragonal crystalline structure of the $CsPbCl_3$ host. Meaningfully, Mn substitution greatly enhances the photoluminescence quantum yields of $CsPbCl_3$ from 5 to 54%. The enhanced emission is attributed to the energy transfer of photoinduced excitons from the $CsPbCl_3$ host to the doped Mn, which facilitates exciton recombination *via* a radiative pathway. The intensity and position of this Mn-related emission are also tunable by altering the experimental parameters, such as reaction temperature and the Pb-to-Mn feed ratio. A light-emitting diode (LED) prototype is further fabricated by employing the as-prepared $CsPb_xMn_{1-x}Cl_3$ QDs as color conversion materials on a commercially available 365 nm GaN LED chip.**

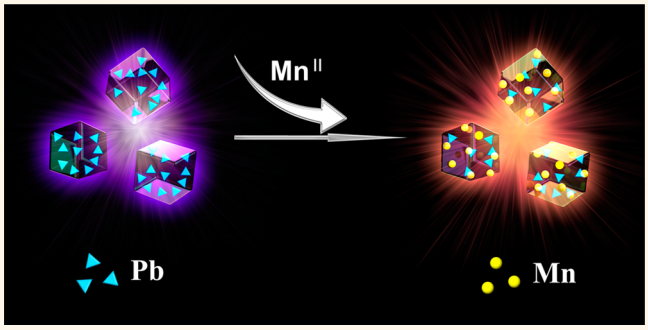

KEYWORDS: *perovskite quantum dots, $CsPb_xMn_{1-x}Cl_3$, low lead, phosphine-free preparation, light-emitting diode*

Perovskite quantum dots (QDs) are promising emitting materials for illumination and display applications because of the low cost, high photoluminescence quantum yields (PLQYs), as well as narrow and tunable emission spectra.[1−12] These advantages make perovskite QDs excellent candidates for fabricating high-performance light-emitting diodes (LEDs).[13−23] The primary perovskite QDs are organic−inorganic hybrid $CH_3NH_3PbX_3$ (X = Cl, Br, I).[2,6,12,24−26] Although the organic−inorganic hybrid perovskite QDs offer the advantages of high efficiencies, low processing temperatures, cost-effectiveness, scalable fabrication, and short decay time similar to that of the intrinsic state of semiconductor materials, they are extremely sensitive to oxygen and moisture.[27−32] Accordingly, fully inorganic $CsPbX_3$ (X = Cl, Br, I) QDs are emerging as a new class of metal halide perovskite QDs, which are less susceptible toward oxygen and moisture than their hybrid counterparts.[33−35] To date, tremendous progress has been achieved in controlling the morphology, size, and halide of $CsPbX_3$ perovskite QDs, which also produce QDs with PL emission tunable from green to red.[36−43] However, the main component of Pb is highly toxic, which causes concern for industrial applications of Pb-based QDs.[44] The replacement of toxic Pb with other nontoxic or less toxic elements is required.

Recently, great efforts have been devoted to preparing lead-free perovskite QDs in colloidal solution.[45,46] The key is to maintain the cubic or tetragonal crystalline structure of the perovskite host.[44,47−49] To our best knowledge, the most successful substitute elements of Pb include Sn and Bi, such as the reported $CsSnX_3$ and $(CH_3NH_3)_3Bi_2Br_9$ perovskite QDs.[45,46] For $(CH_3NH_3)_3Bi_2Br_9$ QDs, they exhibit a PLQY up to 12%, which is much lower than that of Pb-based counterparts.[41−43] Besides, the capability to tune the wavelength of PL emission is also poor.[46] For $CsSnX_3$ QDs, the PLQY is only 0.14%, and toxic tri-*n*-octylphosophine is necessary as a mild reduction with coordinating solvent in the reaction solution to prevent QD aggregation.[45] The as-prepared $CsSnX_3$ QDs are also unstable and lose the emission within a few hours, owing to the intrinsic defect sites and the oxidation process from Sn^{II} to Sn^{IV}.[45] Systematical studies

Received: December 31, 2016
Accepted: January 30, 2017
Published: February 1, 2017

DOI: 10.1021/acsnano.6b08747
ACS Nano 2017, 11, 2239−2247

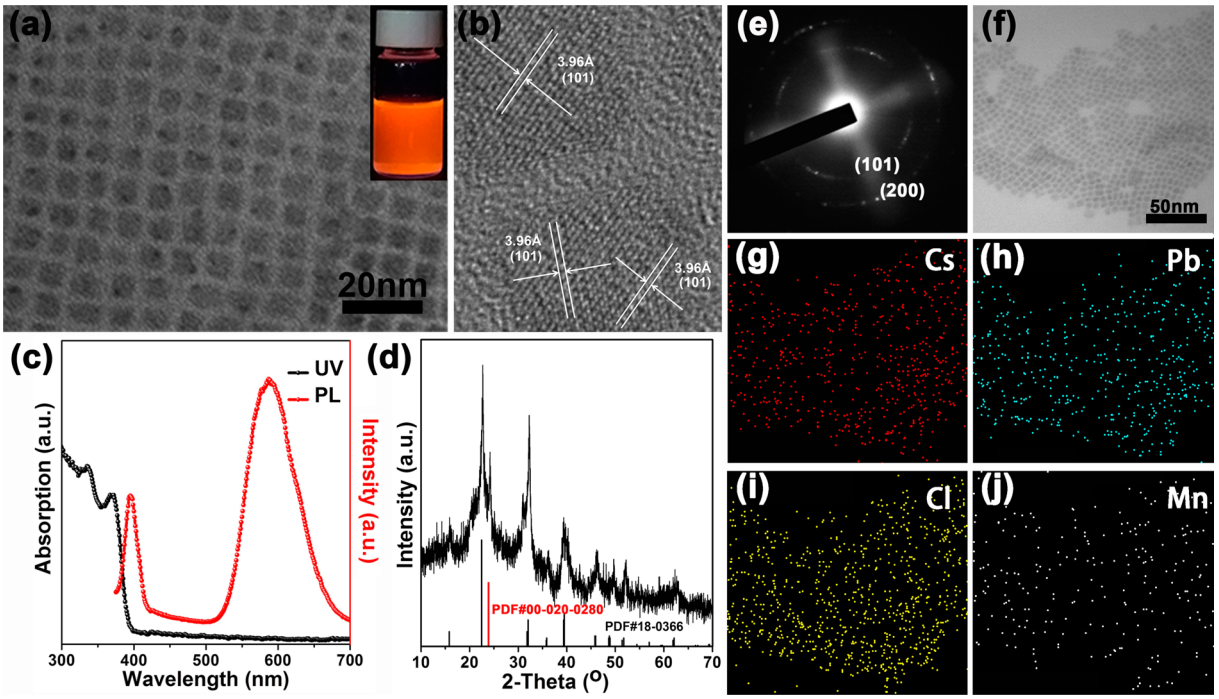

Figure 1. TEM image (a), HRTEM image (b), UV absorption and PL emission spectra (c), XRD pattern and standard diffraction pattern (d), SAED pattern (e), and mapping images (f–j) of $CsPb_{0.54}Mn_{0.46}Cl_3$ QDs. Inset in (a): PL image excited by 365 nm UV light.

reveal that Pb-based perovskite QDs are highly ionic, originating from the high ionic conductivity of Pb.[44] However, the less toxic Sn and Bi do not have the comparative ionic conductivity like Pb. As a result, their high surface defects and large band gap lower the PLQYs and stability.[50]

Since Pb is the key for preserving high PLQYs and stability in perovskite QDs, the partial replacement of Pb with other metals is an alternative route.[51,52] Note that in the previous studies on II–VI semiconductor QDs, the additional transition metal ions are capable of introducing a new exciton transition pathway and alter the emission properties.[53] The mostly used transition metal ions are Cu^{II} and Mn^{II}.[54−58] With respect to the compatibility of cations, Mn^{II} and Pb^{II} possess the same valence state and similar ionic radius.[51] Mn–Cl and Pb–Cl bonds also have similar bond dissociation energy.[51] These permit the partial replacement of Pb in $CsPbCl_3$ QDs with Mn. Our consideration is also supported by the recent success in preparing Mn^{II}-doped $CsPbX_3$ QDs, though the Mn substitution ratio is lower than 10% and the PLQY is lower than that of Pb-based perovskite QDs.[51,52]

In this work, we demonstrate the colloidal preparation of $CsPb_xMn_{1-x}Cl_3$ perovskite QDs with a Mn substitution ratio up to 46%. Besides the reduction of lead content, the as-prepared QDs maintain the tetragonal crystalline structure of the $CsPbCl_3$ host and exhibit strong PL emission of Pb-based perovskite QDs. Mn substitution not only enhances the PLQYs of $CsPbCl_3$ from 5 to 54% but also results in an additional strong emission centered at about 580 nm. This Mn-related emission is attributed to the energy transfer of photoinduced excitons from the $CsPbCl_3$ host to the doped Mn, which facilitates exciton recombination *via* a radiative pathway. The intensity and position of this Mn-related emission are also tunable by altering the Mn substitution ratio. A LED prototype is further fabricated by employing the as-prepared $CsPb_xMn_{1-x}Cl_3$ QDs as color conversion materials.

RESULTS AND DISCUSSION

$CsPb_{0.54}Mn_{0.46}Cl_3$ QDs with Dual-Color Emission. The low-lead perovskite QDs are prepared in colloidal solution by introducing $MnCl_2$ into Pb precursors. In a typical reaction, $MnCl_2$ and $PbCl_2$ are foremost dissolved in a mixture of octadecene, oleylamine, and oleic acid (OA) under vacuum at 120 °C to produce the precursor solution of cations. Subsequently, cesium–oleate solution is rapidly injected into the cation precursor at 210 °C (Supporting Information Figure S1). The reaction solution is kept at 210 °C to maintain the growth of QDs. After purification, the products are dispersed in hexane and characterized. As revealed by transmission electron microscopy (TEM), the as-prepared QDs indicate a cubic morphology with an average size of 6.6 ± 1.0 nm (Figure 1a). The cubic morphology is like $CsPbCl_3$, but the size is much smaller (Figure S2a). High-resolution TEM (HRTEM) observation reveals that the as-prepared QDs have legible crystal lattices with an interplanar distance of 3.96 Å (Figure 1b), which consists of the (101) plane of the tetragonal bulk $CsPbCl_3$ (PDF#18-0366). The selected area electron diffraction (SAED) pattern also indicates that the QDs possess tetragonal crystal structure with corresponding (101) and (200) planes (Figure 1e).[59] The X-ray diffraction (XRD) pattern further confirms that the QDs possess the crystalline structure of tetragonal bulk $CsPbCl_3$ (Figure 1d).[59] In addition, the XRD pattern shows a new diffraction peak at 24.4°, which may result from the presence of Mn^{II} in the $CsPbCl_3$ host and will be discussed later.[51]

The as-prepared QDs indicate good dispersibility in nonpolar solvents, such as hexane and toluene. The hexane solution of the QDs shows an absorption peak at 372 nm (Figure 1c). With 365 nm ultraviolet (UV) irradiation, the QD solution exhibits a bright orange emission (Figure 1a inset). The PL emission spectrum shows dual emission peaks, which centers at 396 and 587 nm, respectively (Figure 1c). The narrow band-

DOI: 10.1021/acsnano.6b08747
ACS Nano 2017, 11, 2239–2247

edge emission with the full width at half-maximum (fwhm) of 12 nm is assigned to the emission of the $CsPbCl_3$ host (Figure S2c),[41] whereas the broad emission band with the fwhm at about 80 nm is probably from the presence of Mn^{II} in $CsPbCl_3$.[51] Energy-dispersive X-ray spectroscopy (EDX) and mapping images further confirm the presence of Mn^{II} in $CsPbCl_3$ (Figure 1f–j). The ratio of Cs, Pb, Mn, and Cl is 1:0.54:0.46:3, revealing the composition of the QDs as $CsPb_{0.54}Mn_{0.46}Cl_3$. To exclude the presence of individual $CsMnCl_3$ in the as-prepared QDs, the products are prepared by injecting cesium–oleate solution into Mn precursors without any Pb. As revealed by TEM, the products are amorphous compounds without PL emission (Figure S3), which do not exist in the purified $CsPb_{0.54}Mn_{0.46}Cl_3$ QDs. On the one hand, this result proves the presence of Mn in the as-prepared QDs. On the other hand, it confirms the importance of Pb for maintaining the framework of perovskite QDs.

$CsPb_xMn_{1-x}Cl_3$ QDs with Tunable Composition and Emission Properties. Similar to the doping of Mn^{II} into II–VI semiconductor QDs,[56−58] the Mn substitution in $CsPb_xMn_{1-x}Cl_3$ QDs is a thermodynamics-controlled process. When the reaction temperature is increased from 150 to 210 °C, the Mn substitution ratio increases from 22 to 46%, corresponding to the composition of $CsPb_{0.78}Mn_{0.22}Cl_3$, $CsPb_{0.73}Mn_{0.27}Cl_3$, $CsPb_{0.62}Mn_{0.38}Cl_3$, and $CsPb_{0.54}Mn_{0.46}Cl_3$, respectively (Table S1 and Figure S4). This means that a high reaction temperature facilitates the replacement of Pb^{II} with Mn^{II}. As revealed by TEM observation, the QDs prepared at different temperature exhibit similar cubic morphology and slight size variation (Figure 2), which indicates that the reaction

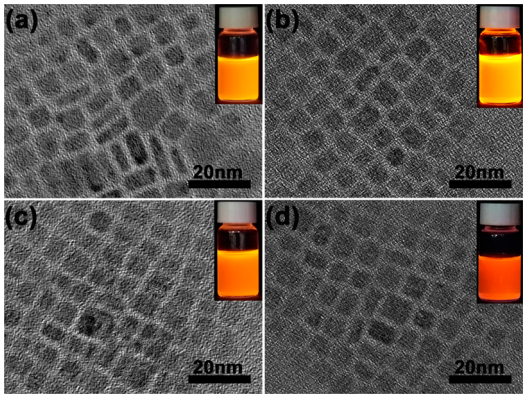

Figure 2. TEM images of the $CsPb_xMn_{1-x}Cl_3$ QDs that are prepared at 150 °C (a), 170 °C (b), 190 °C (c), and 210 °C (d). Insets: Corresponding PL images excited by 365 nm UV light.

temperature does not influence the basic growth process of the $CsPbCl_3$ host. The XRD patterns further confirm that the $CsPb_xMn_{1-x}Cl_3$ QDs prepared at different temperatures possess the same crystalline structure of tetragonal $CsPbCl_3$.[59] These results confirm that high temperature mainly promotes the diffusion of Mn into the $CsPbCl_3$ lattice. Moreover, with increasing temperature, a 0.12° shift of the XRD (101) peak toward higher angle is observed (Figure 3c), which shows the lattice contraction due to the substitution of larger Pb^{II} ions (133 pm) by smaller Mn^{II} ions (97 pm).[51] With increased reaction temperature, a new peak at 24.4° gradually appears, consistent with the (110) lattice plane of hexagonal $CsMnCl_3$ (PDF#00-020-0280, Figure 3c). These results prove the existence of Mn^{II} in the $CsPbCl_3$ host, which may have one

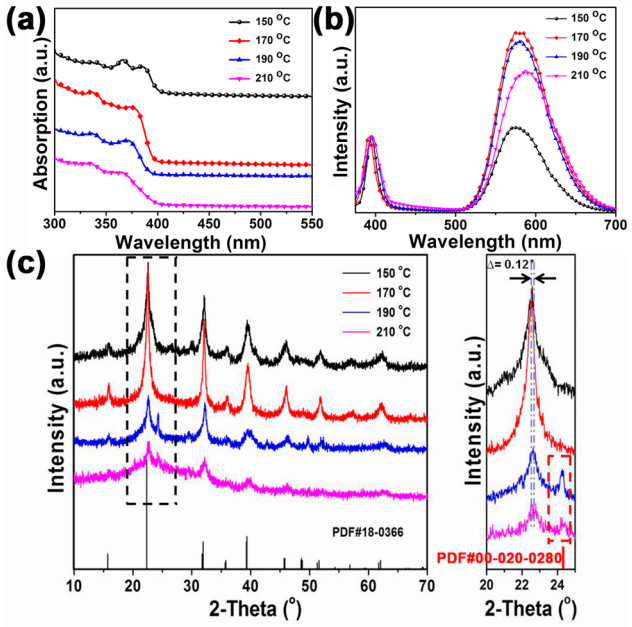

Figure 3. UV–vis absorption (a) and PL emission (b) spectra of the $CsPb_xMn_{1-x}Cl_3$ QDs that are prepared by at 150, 170, 190, and 210 °C. (c) XRD patterns show the diffraction of tetragonal phase $CsPbCl_3$ (PDF#18-0366) and the careful examination of the (101) plane.

form or another, either partially replacing the sites of Pb^{II} in the $CsPbCl_3$ host or just occupying the space between the cations of $CsPbCl_3$. Note that the crystallinity of $CsPb_xMn_{1-x}Cl_3$ QDs also decreases with the increase of reaction temperature and, therefore, the Mn substitution ratio. As more Mn^{II} ions are immersed into the $CsPbCl_3$ lattice and subsequently replace the Pb sites, the framework of $CsPbCl_3$ is partially destroyed.

The $CsPb_xMn_{1-x}Cl_3$ QDs prepared at different temperatures show a slight shift of the UV–vis absorption peaks due to slight changes in QD size (Figure 3a). With increased reaction temperature, the PL emission peak around 580 nm shows a red shift from 575 to 587 nm, which is from the increased Mn^{II} content (Figure 3b and Table S1). The enhanced Mn–Mn interaction causes the energy decrease of Mn^{II}-related emission and, therefore, the red shift of PL emission.[60] The PL emission also shows the trend of intensity variation *versus* reaction temperature, which increases first and then decreases (Figure 3b). The QDs prepared at 170 °C exhibit the strongest PLQY of 54% (Table S1). The PL images of the QD hexane solution with 365 nm UV irradiation indicate a similar trend (Figure 2a–d insets). These results mean that the emission intensity of $CsPb_xMn_{1-x}Cl_3$ QDs relates to both the Mn substitution ratio and the crystallinity of the $CsPbCl_3$ host. Although Mn substitution generates an additional emission around 580 nm, the efficient exciton recombination still depends on the crystallinity of the $CsPbCl_3$ host. In return, it proves the importance of the tetragonal $CsPbCl_3$ framework for preserving a strong emission. The as-prepared QD solution shows good chemical stability, which preserves the crystal structures and emission properties under ambient light and atmospheres for at least 3 months (Figure S5). However, under strong UV exposure, the $CsPb_xMn_{1-x}Cl_3$ QDs show PL decay similar to that of $CsPbCl_3$ (Figure S6).

As mentioned above, reaction temperature greatly influences the Mn substitution ratio in $CsPb_xMn_{1-x}Cl_3$ QDs owing to the

DOI: 10.1021/acsnano.6b08747
ACS Nano 2017, 11, 2239–2247

elevated activity of Mn^{II} ions at high temperature. The substitution of Mn is capable of enhancing emission and influencing the emission color. Combined with the structural and spectral analysis of $CsPb_xMn_{1-x}Cl_3$ QDs, it can be concluded that appropriate Mn substitution benefits the emission of the $CsPbCl_3$ host, which is attributed to the energy transfer of photoinduced excitons from the $CsPbCl_3$ host to the doped Mn^{II}.[52] However, excess Mn substitution will destroy the crystallinity of the $CsPbCl_3$ host, thus reducing the PL.

Note that the activity of Mn^{II} is much lower than that in Pb^{II} in forming $CsPb_xMn_{1-x}Cl_3$ QDs. To increase the Mn^{II} content in the as-prepared QDs, a low Pb-to-Mn feed ratio is necessary. By fixing the reaction temperature at 170 °C, the influence of Pb-to-Mn molar feed ratio is studied. With the decrease of Pb-to-Mn molar feed ratio from 1:1.25, 1:2.5, 1:5, to 1:10, the size of as-prepared QDs gradually decreases (Figure 4). EDX

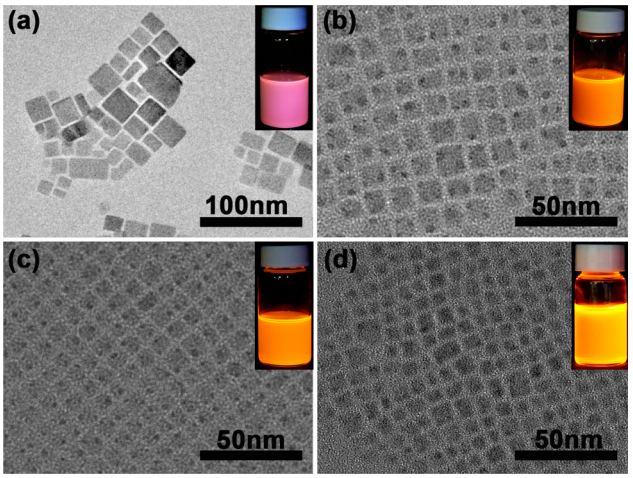

Figure 4. TEM images of the $CsPb_xMn_{1-x}Cl_3$ QDs that are prepared with Pb-to-Mn molar feed ratios of 1:1.25 (a), 1:2.5 (b), 1:5 (c), and 1:10 (d) at 170 °C. Insets: Corresponding PL images excited by 365 nm UV light.

analysis of the as-prepared QDs reveals the composition of $CsPb_{0.98}Mn_{0.02}Cl_3$, $CsPb_{0.96}Mn_{0.04}Cl_3$, $CsPb_{0.90}Mn_{0.10}Cl_3$, and $CsPb_{0.73}Mn_{0.27}Cl_3$, respectively (Figure S7). XRD patterns indicate that the products consist of the crystal structure of tetragonal $CsPbCl_3$ with a 0.1° shift to the higher angle at low Pb-to-Mn ratio,[51] showing a lattice contraction at a high Mn substitution ratio. The aforementioned results are similar to the effect of reaction temperature. Namely, the shift of XRD diffraction peaks is from the increase of Mn^{II} content in the $CsPbCl_3$ host. Due to the decreased size of $CsPb_xMn_{1-x}Cl_3$ QDs, their UV−vis absorption spectra show a gradual blue shift with the decreased Pb-to-Mn molar feed ratio (Figure 5a). Likewise, the narrow PL emission peak around 390 nm also shows a blue shift (Figure 5b). With the emission intensity, an obvious intensity increase is found for the broad emission around 580 nm (Table S2), which is attributed to the enhancement of exciton-to-Mn^{II} energy transfer.[60] Although the Pb-to-Mn ratio influences the Mn substitution ratio, such an effect is less obvious than reaction temperature, which proves that the activity of Mn^{II} ions is more crucial than the ratio in the reaction system.

The influence of heating rate and precursor concentration is also studied. For the heating rate, there is no change in the

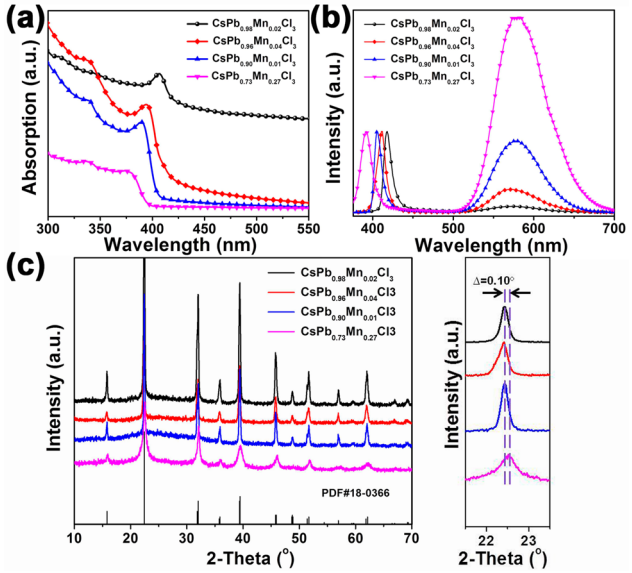

Figure 5. UV−vis absorption (a) and PL emission (b) spectra of the $CsPb_xMn_{1-x}Cl_3$ QDs that are prepared with Pb-to-Mn molar feed ratios of 1:1.25, 1:2.5, 1:5, and 1:10 at 170 °C. (c) XRD patterns show the diffraction of tetragonal phase $CsPbCl_3$ (PDF#18-0366) and the careful examination of the (101) plane.

morphology and emission properties of the as-prepared $CsPb_xMn_{1-x}Cl_3$ QDs (Figure S8). This is mainly attributed to the rapid nucleation and growth of the perovskite QDs with the injection of Cs−OA solution into cation precursors. The precursor concentration indeed affects the morphology and PL properties of the as-prepared QDs. By fixing the 1:10 Pb-to-Mn feed ratio and the reaction temperature of 170 °C, the influence of precursor concentration is revealed. In general, the as-prepared QDs exhibit the most uniform size distribution and strongest emission with the precursor concentration of 0.02 mol/L referring to Pb (Figure S9). When the precursor concentration is reduced to 0.01 mol/L, the QDs' size and emission intensity remain the same. As the concentration increases to 0.04 mol/L, an inhomogeneous size distribution and obvious emission decrease are found (Figure S9d). This is attributed to the formation of excess nucleus at a high precursor concentration after the injection of Cs−OA solution.[61] The remaining precursors are not enough to support a homogeneous growth of QD ensembles, which results in the inhomogeneous size distribution of QDs. The inhomogeneous QD growth also leads to a poor arrangement of the atoms of QDs and lowers the emission intensity.

By combining the influence of experimental variables, we produced a series of $CsPb_xMn_{1-x}Cl_3$ QDs with tunable composition and emission properties (Table 1 and Scheme 1). The Mn substitution ratio is up to 46%, while the PLQY is up to 54%. The emission peak can be tuned from 569 to 587 nm.

Emission Mechanism of $CsPb_xMn_{1-x}Cl_3$ QDs. To further reveal the mechanism of Mn^{II}-induced emission, the fluorescent lifetimes of $CsPb_xMn_{1-x}Cl_3$ QDs are investigated. The QDs exhibit two lifetimes, 13.9 ns at 390 nm and 1.6 ms at 580 nm (Figure 6a,b). The difference in the lifetimes implies that the origin of the two emission peaks is different. The lifetime at 390 nm consists of the decay time of the previously reported emission of the $CsPbCl_3$ host.[41] By combining the composition and spectral analysis of $CsPb_xMn_{1-x}Cl_3$ QDs, the long decay

DOI: 10.1021/acsnano.6b08747
ACS Nano 2017, 11, 2239−2247

Table 1. Summary of the Fluorescent Tunability of $CsPb_xMn_{1-x}Cl_3$ QDs[a]

Reaction Temperature (°C)	Pb-to-Mn molar feed ratio	Pb-precursor concentration (mol/L)	Element composition	PL images	PL emission peak position (nm)	PLQYs (%)
150	1:2.5	0.02	$CsPb_{0.97}Mn_{0.03}Cl_3$		569	5
170	1:10	0.02	$CsPb_{0.73}Mn_{0.27}Cl_3$		579	54
190	1:2.5	0.01	$CsPb_{0.94}Mn_{0.06}Cl_3$		574	22
190	1:10	0.02	$CsPb_{0.62}Mn_{0.38}Cl_3$		582	36
210	1:5	0.01	$CsPb_{0.87}Mn_{0.13}Cl_3$		575	43
210	1:10	0.02	$CsPb_{0.54}Mn_{0.46}Cl_3$		587	17

[a]By altering the reaction temperature, Pb-to-Mn molar feed ratio, and precursor concentration, the PL emission peak is tunable from 569 to 587 nm, and the PLQY is tunable from 5 to 54%. The corresponding PL images are excited by 365 nm UV light.

Scheme 1. Schematic Illustration of the Fluorescent Tunability of $CsPb_xMn_{1-x}Cl_3$ QDs by Alerting the Mn-to-Pb Molar Feed Ratio and Reaction Temperature[a]

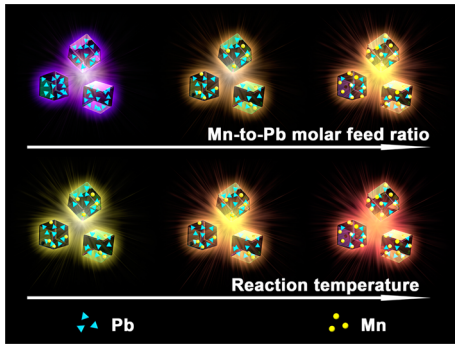

[a]The corresponding TEM and fluorescent images are shown in Figure 2 and Figure 4.

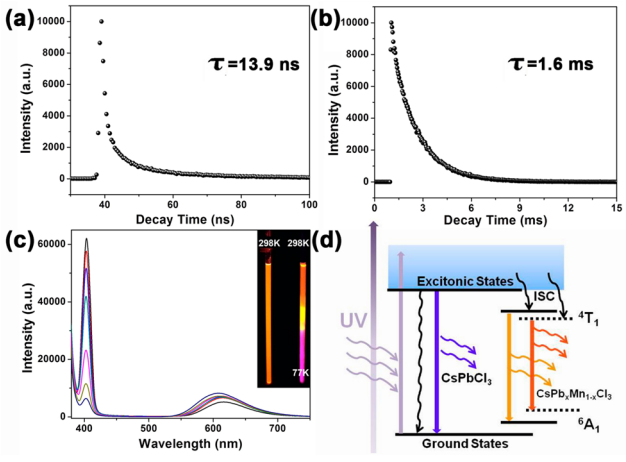

Figure 6. (a) Fluorescent lifetime of the $CsPbCl_3$ NPLs at 390 nm. (b) Fluorescent lifetime of $CsPb_{0.73}Mn_{0.27}Cl_3$ QDs at 580 nm. (c) Temperature-dependent emission spectra of the $CsPb_{0.73}Mn_{0.27}Cl_3$ QDs. (d) Energy levels and fluorescent mechanism of $CsPb_xMn_{1-x}Cl_3$ QDs, where ISC represents intersystem crossing.

time of the broad emission peak around 580 nm is assigned to emission from excitons-to-Mn^{II} energy transfer according to the emission properties of Mn^{II}-doped II–VI semiconductor QDs.[52,56−58,60] To further confirm the origin of the double band emission, the PL excitation spectra of $CsPb_xMn_{1-x}Cl_3$ and $CsPbCl_3$ are compared (Figure S10). The PL excitation spectra show the same three excitation peaks at 337, 352, and 370 nm. Monitored at the same wavelength, the PL excitation spectra of $CsPb_xMn_{1-x}Cl_3$ and $CsPbCl_3$ are almost the same (Figure S10a,c), proving that the initial form of the excitons in $CsPbCl_3$ and $CsPb_xMn_{1-x}Cl_3$ is similar. This is consistent with the proposed mechanism of Mn^{II}-related emission through the exciton energy transfer from the $CsPbCl_3$ host to the doped Mn^{II} ions. Also, the excitation-dependent PL spectra indicate that the dual emission peaks have no shift by alerting the excitation wavelength from 340 to 380 nm. The independence of the PL spectra on excitation wavelength confirms the single source of the dual emission, namely, the exciton recombination of the $CsPbCl_3$ host (Figure S11).

To confirm this consideration, the temperature-dependent emission of $CsPb_xMn_{1-x}Cl_3$ QDs is tested and analyzed. At 77 K, the two emission peaks exhibit different variation (Figure 6c). The position of the emission peak around 390 nm is almost fixed, whereas the emission intensity greatly increases. In comparison, the position of the emission peak around 580 nm shows a red shift with a slight decline of emission intensity. Such variation is consistent with the property of the $CsPbCl_3$ host emission and the emission of Mn^{II}-induced energy transfer.[59,60]

According to the aforementioned results, the emission model of $CsPb_xMn_{1-x}Cl_3$ QDs is schemed in Figure 6d. Excited by 365 nm radiation, the $CsPbCl_3$ host absorbs the energy and emits a 390 nm emission *via* the radiative recombination of excitons between the ground state and the excited state of $CsPbCl_3$. Besides the radiative recombination, a nonradiative relaxation process also exists, which leads to energy loss through hole traps or electron traps. As a result, the PLQY of $CsPbCl_3$ QDs is below 5%. The Mn substitution generates a new recombination pathway of excitons with the property of exciton-to-Mn^{II} energy transfer, which enables the transition from one excited state to the other with thermally actived electrons. Only the excitons possessing enough thermal activition energy will experience an intersystem crossing (ISC) process and finally emit the 580 nm emission, showing the new excitons' recombination pathway of d–d transition of

DOI: 10.1021/acsnano.6b08747
ACS Nano 2017, 11, 2239−2247

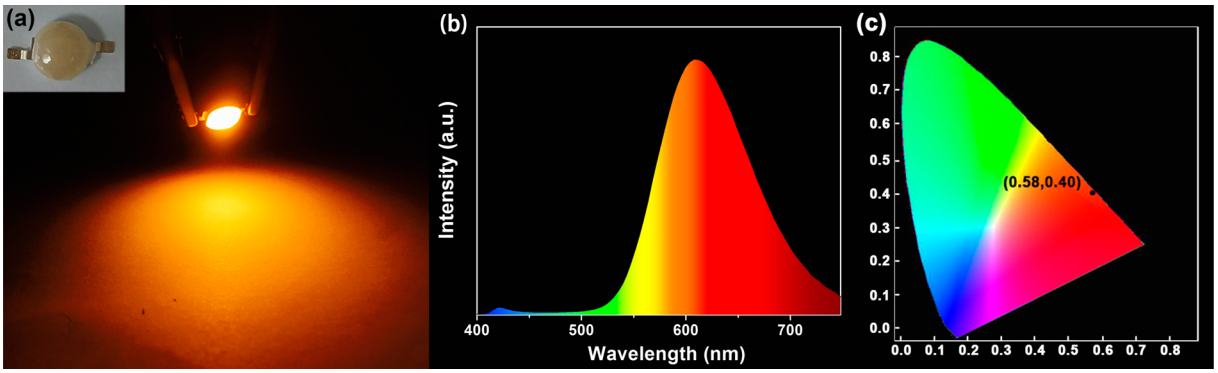

Figure 7. Fluorescent image (a), PL emission spectrum (b), and CIE chromaticity coordinate (c) of the LED from $CsPb_xMn_{1-x}Cl_3$ QDs. Inset: Optical image of the LED.

Mn^{II} ions, namely, $^4T_1-^6A_1$ transition.[60] From Mn^{II} doping, the energy transfer of the photoinduced excitons from the $CsPbCl_3$ host to the doped Mn^{II} ions facilitates the exciton recombination *via* a radiative pathway and enhances the PL intensity.

This model is also helpful to explain the long fluorescent lifetime of 1.6 ms *via* the ISC process (Figure 6b). In addition, the temperature-dependent emission is determined by nonradiative recombination of excitons and ISC process according to this model. On the one hand, with decreased temperature, the nonradiative relaxation process is greatly restricted and therefore the intensity of $CsPbCl_3$ host emission is enhanced (Figure 6c). On the other hand, the decreased thermodynamic energy of electrons makes it difficult to undergo the ISC process, thus suppressing the exciton-to-Mn^{II} energy transfer (Figure 6c). With respect to the emission color, the decreased temperature slightly reduces the energy level of $^4T_1-^6A_1$ transition but enhances the Mn−Mn interaction. As a result, the Mn^{II}-related emission shows a red shift.

LEDs from $CsPb_xMn_{1-x}Cl_3$ QDs. Because the as-prepared $CsPb_xMn_{1-x}Cl_3$ QDs possess high PLQYs up to 54% and good PL stability, they are tested as the color conversion materials for fabricating LEDs. For example, $CsPb_{0.73}Mn_{0.27}Cl_3$ QDs with orange-red emission are mixed with curable resin, coated on a commercially available 365 nm GaN LED chip, and cured under UV light for 2 min (Methods section). The LED device exhibits bright orange-red emission with the color coordinate of (0.58, 0.40) (Figure 7a,c). The corresponding emission spectrum is shown in Figure 7b. The luminous efficiency of the device is 2.2 lm/W, which is not high but at an acceptable level for perovskite QD-based LED devices. After continuously working at the constant voltage of 3.5 V for 200 h, the emission color, emission intensity, and the color coordinates of the device are unchanged (Figure S12).

CONCLUSIONS

In summary, $CsPb_xMn_{1-x}Cl_3$ perovskite QDs with a high Mn substitution ratio are prepared through a phosphine-free hot-injection method. The Mn substitution ratio is up to 46%, and the PLQY is up to 54%. Besides the emission of the $CsPbCl_3$ host, the as-prepared QDs exhibit a strong Mn^{II}-related emission, which is attributed to the energy transfer of photoinduced excitons from the $CsPbCl_3$ host to the doped Mn^{II} ions. Such a process facilitates the exciton recombination *via* a radiative pathway. The as-prepared $CsPb_xMn_{1-x}Cl_3$ QDs are further employed as the color conversion materials on a commercially available 365 nm GaN LED chip for fabricating LEDs. Since the ratio of toxic Pb in perovskite QDs is greatly decreased, the current strategy is considered to promote the practical applications of perovskite QDs in illumination and display.

METHODS

Materials. Cs_2CO_3 (99.9%), $PbCl_2$ (99.9%), octadecene (ODE, technical grade, 90%), oleic acid (technical grade, 90%), and oleylamine (OLA, technical grade, 90%) were purchased from Aldrich. $MnCl_2$ (99.9%) was purchased from Aladdin Industrial Corporation, China. Hexane and ethyl acetate were purchased from Beijing Chemical Reagent Ltd., China, and used as received without further purification.

Preparation of Cesium−Oleate Solution. Cesium−oleate solution was prepared according to the approach reported by Protesescu *et al.*[41] In brief, 0.4 g of Cs_2CO_3, 1.2 mL of OA, and 15 mL of ODE were loaded in a three-neck flask and degassed under vacuum at 120 °C for 1 h, followed by heating at 150 °C under N_2 atmosphere until all Cs_2CO_3 reacted with OA.

Preparation of $CsPbCl_3$ NPLs. Fifty-two milligrams of $PbCl_2$ and 5 mL of ODE were loaded in a 50 mL three-neck flask and dried under vacuum for 1 h at 120 °C. Dried 2 mL of OLA and 2 mL of OA were injected at 120 °C under N_2. After the complete dissolution of $PbCl_2$, the temperature was increased to 170 °C. Finally, 0.6 mL of hot 150 °C Cs−oleate solution was quickly injected, and the reaction mixture was cooled by a water bath.

Preparation of $CsPb_xMn_{1-x}Cl_3$ QDs. $PbCl_2$ and $MnCl_2$ with a specific molar ratio were mixed with 5 mL of ODE in a 50 mL three-neck flask and dried under vacuum for 1 h at 120 °C. Dried 2 mL of OLA and 2 mL of OA were injected at 120 °C under N_2. After the complete dissolution of $PbCl_2$ and $MnCl_2$, the temperature was increased to 150, 170, 190, and 210 °C. Then, 0.6 mL of hot 150 °C Cs−oleate solution was quickly injected, and the reaction mixture was cooled by a water bath.

Purification. The $CsPbCl_3$ NPLs and $CsPb_xMn_{1-x}Cl_3$ QDs were extracted from the crude solution by centrifuging at 8500 rpm for 5 min to discard the supernatant containing unreacted precursor and byproducts. After that, 5 mL of hexane was added into the precipitates to disperse, and subsequently, 10 mL of ethyl acetate was used to induce aggregation, followed by centrifugation at 8500 rpm for 5 min. After centrifugation, the supernatant was discarded and the precipitates were redispersed in hexane, forming a stable colloidal solution.

Fabrication of LEDs from $CsPb_xMn_{1-x}Cl_3$ QDs. Commercially available GaN LED chips without phosphor coating were purchased from Advanced Optoelectronic Technology Inc. The emission of the GaN LED chips centered at 365 nm, and the operating voltage was 4.0 V. In the preparation of the color conversion layer, $CsPb_xMn_{1-x}Cl_3$ QDs were foremost milled to a fine powder and mixed with the curable resin according to our previous method and put in a vacuum chamber to remove bubbles.[62] After that, the mixtures were used to fill

DOI: 10.1021/acsnano.6b08747
ACS Nano 2017, 11, 2239−2247

the cup-shaped void of an LED chip. After being cured under UV light for 2 min, the LEDs from $CsPb_xMn_{1-x}Cl_3$ QDs were fabricated.

Characterization. UV−visible absorption spectra were obtained using a Shimadzu 3100 UV−vis spectrophotometer. Fluorescence spectroscopy was performed with a Shimadzu RF-5301 PC spectrophotometer. Transmission electron microscopy images and selected area electron diffraction patterns were recorded using a H-800 electron microscope (Hitachi) at an acceleration voltage of 200 kV with a charged-coupled device camera. HRTEM images were recorded using a JEM-2100F electron microscope (JEOL) at 200 kV. An EDX detector coupled with a XL30 ESEM FEG scanning electron microscope (FEI) was used for elemental analysis. Inductively coupled plasma was performed with an OPTIMA 3300 DV analyzer (PerkinElmer). X-ray diffraction was carried out on a X-ray diffractometer (Rigaku) using Cu K radiation (λ = 1.5418 Å). The absolute QYs of QDs were measured on an Edinburgh FLS920 (excited at 365 nm) instrument equipped with an integrating sphere. The luminescence decay curves were measured on a FLS920 spectrofluorometer. The spectrum of the LED was measured under ambient conditions at room temperature by combining a Spectra scan PR-650 spectrophotometer with an integrating sphere and a computer-controlled direct current power. The color of the light was identified by the CIE (Commission Internationale de L'Eclairage 1931) calorimeter system.

ASSOCIATED CONTENT

Supporting Information

The Supporting Information is available free of charge on the ACS Publications website at DOI: 10.1021/acsnano.6b08747.

Additional schematic illustration, TEM images, XRD pattern, absorption spectrum, EDX analysis, PL emission and excitation spectra, and PLQYs of $CsPb_xMn_{1-x}Cl_3$ QDs and $CsPbCl_3$ NPLs (PDF)

AUTHOR INFORMATION

Corresponding Author

*E-mail: hao_zhang@jlu.edu.cn.

ORCID

Yi Liu: 0000-0003-0548-6073

Hao Zhang: 0000-0002-2373-1100

Bai Yang: 0000-0002-3873-075X

Author Contributions

H.Z. proposed and supervised the project. H.Z., H.W.L., Z.N.W., Y.L., and B.Y. designed and performed the experiments and co-wrote the paper. J.R.S., D.Y., H.G., and W.L.Y. participated in most experiments. All authors discussed the results and commented on the manuscript.

Notes

The authors declare no competing financial interest.

ACKNOWLEDGMENTS

This work was supported by the National Key Research and Development program of China (2016YFB0401701), NSFC (51425303, 21404015, 21374042), the 973 Program of China (2014CB643503), and the Special Project from MOST of China.

REFERENCES

(1) Pan, J.; Quan, L. N.; Zhao, Y.; Peng, W.; Murali, B.; Sarmah, S. P.; Yuan, M.; Sinatra, L.; Alyami, N. M.; Liu, J.; Yassitepe, E.; Yang, Z.; Voznyy, O.; Comin, R.; Hedhili, M. N.; Mohammed, O. F.; Lu, Z. H.; Kim, D. H.; Sargent, E. S.; Bakr, O. M. Highly Efficient Perovskite-Quantum-Dot Light-Emitting Diodes by Surface Engineering. *Adv. Mater.* **2016**, *28*, 8718−8725.

(2) Zhang, F.; Zhong, H.; Chen, C.; Wu, X.; Hu, X.; Huang, H.; Han, J.; Zou, B.; Dong, Y. Brightly Luminescent and Color-Tunable Colloidal $CH_3NH_3PbX_3$ (X = Br, I, Cl) Quantum Dots: Potential Alternatives for Display Technology. *ACS Nano* **2015**, *9*, 4533−4542.

(3) Li, X.; Yu, D.; Cao, F.; Gu, Y.; Wei, Y.; Wu, Y.; Song, J.; Zeng, H. Healing All-Inorganic Perovskite Films *via* Recyclable Dissolution-Recrystallization for Compact and Smooth Carrier Channels of Optoelectronic Devices with High Stability. *Adv. Funct. Mater.* **2016**, *26*, 5903−5912.

(4) Zhang, X.; Xu, B.; Zhang, J.; Gao, Y.; Zheng, Y.; Wang, K.; Sun, X. W. All-Inorganic Perovskite Nanocrystals for High-Efficiency Light Emitting Diodes: Dual-Phase $CsPbBr_3$-$CsPb_2Br_5$ Composites. *Adv. Funct. Mater.* **2016**, *26*, 4595−4600.

(5) Nozik, A. J. Nanophotonics: Making the Most of Photons. *Nat. Nanotechnol.* **2009**, *4*, 548−549.

(6) Tan, Z.-K.; Moghaddam, R. S.; Lai, M. L.; Docampo, P.; Higler, R.; Deschler, F.; Price, M.; Sadhanala, A.; Pazos, L. M.; Credgington, D.; Hanusch, F.; Bein, T.; Snaith, H. J.; Friend, R. H. Bright Light-Emitting Diodes Based on Organometal Halide Perovskite. *Nat. Nanotechnol.* **2014**, *9*, 687−692.

(7) Yoon, H. C.; Kang, H.; Lee, S.; Oh, J. H.; Yang, H.; Do, Y. R. Study of Perovskite QD Down-Converted LEDs and Six-Color White LEDs for Future Displays with Excellent Color Performance. *ACS Appl. Mater. Interfaces* **2016**, *8*, 18189−18200.

(8) Zhang, X.; Wang, H.-C.; Tang, A.-C.; Lin, S.-Y.; Tong, H.-C.; Chen, C.-Y.; Lee, Y.-C.; Tsai, T.-L.; Liu, R.-S. Robust and Stable Narrow-Band Green Emitter: An Option for Advanced Wide-Color-Gamut Backlight Display. *Chem. Mater.* **2016**, *28*, 8493−8497.

(9) Zhang, X.; Lin, H.; Huang, H.; Reckmeier, C.; Zhang, Y.; Choy, W. C. H.; Rogach, A. L. Enhancing the Brightness of Cesium Lead Halide Perovskite Nanocrystal Based Green Light-Emitting Devices through the Interface Engineering with Perfluorinated Ionomer. *Nano Lett.* **2016**, *16*, 1415−1420.

(10) De Roo, J.; Ibáñez, M.; Geiregat, P.; Nedelcu, G.; Walravens, W.; Maes, J.; Martins, J. C.; Van Driessche, I.; Kovalenko, M. V.; Hens, Z. Highly Dynamic Ligand Binding and Light Absorption Coefficient of Cesium Lead Bromide Perovskite Nanocrystals. *ACS Nano* **2016**, *10*, 2071−2081.

(11) Park, Y.-S.; Guo, S.; Makarov, N. S.; Klimov, V. I. Room Temperature Single-Photon Emission from Individual Perovskite Quantum Dots. *ACS Nano* **2015**, *9*, 10386−10393.

(12) Veldhuis, S. A.; Boix, P. P.; Yantara, N.; Li, M.; Sum, T. C.; Mathews, N.; Mhaisalkar, S. G. Perovskite Materials for Light-Emitting Diodes and Lasers. *Adv. Mater.* **2016**, *28*, 6804−6834.

(13) Xing, J.; Yan, F.; Zhao, Y.; Chen, S.; Yu, H.; Zhang, Q.; Zeng, R.; Demir, H. V.; Sun, X.; Huan, A.; Xiong, Q. High-Efficiency Light-Emitting Diodes of Organometal Halide Perovskite Amorphous Nanoparticles. *ACS Nano* **2016**, *10*, 6623−6630.

(14) Li, X.; Wu, Y.; Zhang, S.; Cai, B.; Gu, Y.; Song, J.; Zeng, H. $CsPbX_3$ Quantum Dots for Lighting and Displays: Room-Temperature Synthesis, Photoluminescence Superiorities, Underlying Origins and White Light-Emitting Diodes. *Adv. Funct. Mater.* **2016**, *26*, 2435−2445.

(15) Meyns, M.; Perálvarez, M.; Heuer-Jungemann, A.; Hertog, W.; Ibáñez, M.; Nafria, R.; Genç, A.; Arbiol, J.; Kovalenko, M. V.; Carreras, J.; Cabot, A.; Kanaras, A. G. Polymer-Enhanced Stability of Inorganic Perovskite Nanocrystals and Their Application in Color Conversion LEDs. *ACS Appl. Mater. Interfaces* **2016**, *8*, 19579−19586.

(16) Wei, Z.; Perumal, A.; Su, R.; Sushant, S.; Xing, J.; Zhang, Q.; Tan, S. T.; Demir, H. V.; Xiong, Q. Solution-Processed Highly Bright and Durable Cesium Lead Halide Perovskite Light-Emitting Diodes. *Nanoscale* **2016**, *8*, 18021−18026.

(17) Wang, Y.; Li, X.; Song, J.; Xiao, L.; Zeng, H.; Sun, H. All-Inorganic Colloidal Perovskite Quantum Dots: A New Class of Lasing Materials with Favorable Characteristics. *Adv. Mater.* **2015**, *27*, 7101−7108.

(18) Li, G.; Tan, Z.-K.; Di, D.; Lai, M. L.; Jiang, L.; Lim, J. H.-W.; Friend, R. H.; Greenham, N. C. Efficient Light-Emitting Diodes Based

DOI: 10.1021/acsnano.6b08747
ACS Nano 2017, 11, 2239−2247

on Nanocrystalline Perovskite in a Dielectric Polymer Matrix. *Nano Lett.* **2015**, *15*, 2640−2644.
(19) Pathak, S.; Sakai, N.; Wisnivesky Rocca Rivarola, F.; Stranks, S. D.; Liu, J.; Eperon, G. E.; Ducati, C.; Wojciechowski, K.; Griffiths, J. T.; Haghighirad, A. A.; Pellaroque, A.; Friend, R. H.; Snaith, H. J. Perovskite Crystals for Tunable White Light Emission. *Chem. Mater.* **2015**, *27*, 8066−8075.
(20) Song, J.; Li, J.; Li, X.; Xu, L.; Dong, Y.; Zeng, H. Quantum Dot Light-Emitting Diodes Based on Inorganic Perovskite Cesium Lead Halides ($CsPbX_3$). *Adv. Mater.* **2015**, *27*, 7162−7167.
(21) Wang, H.-C.; Lin, S.-Y.; Tang, A.-C.; Singh, B. P.; Tong, H.-C.; Chen, C.-Y.; Lee, Y.-C.; Tsai, T.-L.; Liu, R.-S. Mesoporous Silica Particles Integrated with All-Inorganic $CsPbBr_3$ Perovskite Quantum-Dot Nanocomposites (MP-PQDs) with High Stability and Wide Color Gamut Used for Backlight Display. *Angew. Chem., Int. Ed.* **2016**, *55*, 7924−7929.
(22) Cho, H.; Jeong, S.-H.; Park, M.-H.; Kim, Y.-H.; Wolf, C.; Lee, C.-L.; Heo, J. H.; Sadhanala, A.; Myoung, N.; Yoo, S.; Im, S. H.; Friend, R. H.; Lee, T.-W. Overcoming the Electroluminescence Efficiency Limitations of Perovskite Light-Emitting Diodes. *Science* **2015**, *350*, 1222−1225.
(23) Li, J.; Xu, L.; Wang, T.; Song, J.; Chen, J.; Xue, J.; Dong, Y.; Cai, B.; Shan, Q.; Han, B.; Zeng, H. 50-Fold EQE Improvement up to 6.27% of Solution-Processed All-Inorganic Perovskite $CsPbBr_3$ QLEDs *via* Surface Ligand Density Control. *Adv. Mater.* **2017**, DOI: 10.1002/adma.201603885.
(24) Huang, S.; Li, Z.; Kong, L.; Zhu, N.; Shan, A.; Li, L. Enhancing the Stability of $CH_3NH_3PbBr_3$ Quantum Dots by Embedding in Silica Spheres Derived from Tetramethyl Orthosilicate in "Waterless" Toluene. *J. Am. Chem. Soc.* **2016**, *138*, 5749−5752.
(25) Luo, B.; Pu, Y.-C.; Lindley, S. A.; Yang, L.; Lu, L.; Li, Y.; Li, X.; Zhang, J. Z. Organolead Halide Perovskite Nanocrystals: Branched Capping Ligands Control Crystal Size and Stability. *Angew. Chem., Int. Ed.* **2016**, *55*, 8864−8868.
(26) Kim, Y.-H.; Cho, H.; Heo, J. H.; Kim, T.-S.; Myoung, N.; Lee, C.-L.; Im, S. H.; Lee, T.-W. Multicolored Organic/Inorganic Hybrid Perovskite Light-Emitting Diodes. *Adv. Mater.* **2015**, *27*, 1248−1254.
(27) Ling, Y.; Yuan, Z.; Tian, Y.; Wang, X.; Wang, J. C.; Xin, Y.; Hanson, K.; Ma, B.; Gao, H. Bright Light-Emitting Diodes Based on Organometal Halide Perovskite Nanoplatelets. *Adv. Mater.* **2016**, *28*, 305−311.
(28) Deng, W.; Xu, X.; Zhang, X.; Zhang, Y.; Jin, X.; Wang, L.; Lee, S.-T.; Jie, J. Organometal Halide Perovskite Quantum Dot Light-Emitting Diodes. *Adv. Funct. Mater.* **2016**, *26*, 4797−4802.
(29) Teunis, M. B.; Lawrence, K. N.; Dutta, P.; Siegel, A. P.; Sardar, R. Pure White-Light Emitting Ultrasmall Organic−Inorganic Hybrid Perovskite Nanoclusters. *Nanoscale* **2016**, *8*, 17433−17439.
(30) Gonzalez-Carrero, S.; Galian, R. E.; Pérez-Prieto, J. Maximizing the Emissive Properties of $CH_3NH_3PbBr_3$ Perovskite Nanoparticles. *J. Mater. Chem. A* **2015**, *3*, 9187−9193.
(31) Huang, H.; Susha, A. S.; Kershaw, S. V.; Hung, T. F.; Rogach, A. L. Control of Emission Color of High Quantum Yield $CH_3NH_3PbBr_3$ Perovskite Quantum Dots by Precipitation Temperature. *Adv. Sci.* **2015**, *2*, 1500194−1500198.
(32) Schmidt, L. C.; Pertegás, A.; González-Carrero, S.; Malinkiewicz, O.; Agouram, S.; Minguez Espallargas, G.; Bolink, H. J.; Galian, R. E.; Pérez-Prieto, J. Nontemplate Synthesis of $CH_3NH_3PbBr_3$ Perovskite Nanoparticles. *J. Am. Chem. Soc.* **2014**, *136*, 850−853.
(33) Swarnkar, A.; Chulliyil, R.; Ravi, V. K.; Irfanullah, M.; Chowdhury, A.; Nag, A. Colloidal $CsPbBr_3$ Perovskite Nanocrystals: Luminescence beyond Traditional Quantum Dots. *Angew. Chem., Int. Ed.* **2015**, *54*, 15424−15428.
(34) Tong, Y.; Bladt, E.; Aygüler, M. F.; Manzi, A.; Milowska, K. Z.; Hintermayr, V. A.; Docampo, P.; Bals, S.; Urban, A. S.; Polavarapu, L.; Feldmann, J. Highly Luminescent Cesium Lead Halide Perovskite Nanocrystals with Tunable Composition and Thickness by Ultrasonication. *Angew. Chem., Int. Ed.* **2016**, *55*, 13887−13892.
(35) Kulbak, M.; Cahen, D.; Hodes, G. How Important Is the Organic Part of Lead Halide Perovskite Photovoltaic Cells? Efficient $CsPbBr_3$ Cells. *J. Phys. Chem. Lett.* **2015**, *6*, 2452−2456.
(36) Akkerman, Q. A.; Motti, S. G.; Srimath Kandada, A. R.; Mosconi, E.; D'Innocenzo, V.; Bertoni, G.; Marras, S.; Kamino, B. A.; Miranda, L.; De Angelis, F. D.; Petrozza, A.; Prato, M.; Manna, L. Solution Synthesis Approach to Colloidal Cesium Lead Halide Perovskite Nanoplatelets with Monolayer-Level Thickness Control. *J. Am. Chem. Soc.* **2016**, *138*, 1010−1016.
(37) Sun, S.; Yuan, D.; Xu, Y.; Wang, A.; Deng, Z. Ligand-Mediated Synthesis of Shape-Controlled Cesium Lead Halide Perovskite Nanocrystals *via* Reprecipitation Process at Room Temperature. *ACS Nano* **2016**, *10*, 3648−3657.
(38) Pan, A.; He, B.; Fan, X.; Liu, Z.; Urban, J. J.; Alivisatos, A. P.; He, L.; Liu, Y. Insight into the Ligand-Mediated Synthesis of Colloidal $CsPbBr_3$ Perovskite Nanocrystals: The Role of Organic Acid, Base, and Cesium Precursors. *ACS Nano* **2016**, *10*, 7943−7954.
(39) Bekenstein, Y.; Koscher, B. A.; Eaton, S. W.; Yang, P.; Alivisatos, A. P. Highly Luminescent Colloidal Nanoplates of Perovskite Cesium Lead Halide and Their Oriented Assemblies. *J. Am. Chem. Soc.* **2015**, *137*, 16008−16011.
(40) Nedelcu, G.; Protesescu, L.; Yakunin, S.; Bodnarchuk, M. I.; Grotevent, M. J.; Kovalenko, M. V. Fast Anion-Exchange in Highly Luminescent Nanocrystals of Cesium Lead Halide Perovskites ($CsPbX_3$, X = Cl, Br, I). *Nano Lett.* **2015**, *15*, 5635−5640.
(41) Protesescu, L.; Yakunin, S.; Bodnarchuk, M. I.; Krieg, F.; Caputo, R.; Hendon, C. H.; Yang, R. X.; Walsh, A.; Kovalenko, M. V. Nanocrystals of Cesium Lead Halide Perovskites ($CsPbX_3$, X = Cl, Br, and I): Novel Optoelectronic Materials Showing Bright Emission with Wide Color Gamut. *Nano Lett.* **2015**, *15*, 3692−3696.
(42) Akkerman, Q. A.; D'Innocenzo, V.; Accornero, S.; Scarpellini, A.; Petrozza, A.; Prato, M.; Manna, L. Tuning the Optical Properties of Cesium Lead Halide Perovskite Nanocrystals by Anion Exchange Reactions. *J. Am. Chem. Soc.* **2015**, *137*, 10276−10281.
(43) Li, X.; Cao, F.; Yu, D.; Chen, J.; Sun, Z.; Shen, Y.; Zhu, Y.; Wang, L.; Wei, Y.; Wu, Y.; Zeng, H. All Inorganic Halide Perovskites Nanosystem: Synthesis, Structural Features, Optical Properties and Optoelectronic Applications. *Small* **2017**, 1603996.
(44) Zhang, Y.; Liu, J.; Wang, Z.; Xue, Y.; Ou, Q.; Polavarapu, L.; Zheng, J.; Qi, X.; Bao, Q. Synthesis, Properties, and Optical Applications of Low-Dimensional Perovskites. *Chem. Commun.* **2016**, *52*, 13637−13655.
(45) Jellicoe, T. C.; Richter, J. M.; Glass, H. F. J.; Tabachnyk, M.; Brady, R.; Dutton, S. E.; Rao, A.; Friend, R. H.; Credgington, D.; Greenham, N. C.; Böhm, M. L. Synthesis and Optical Properties of Lead-Free Cesium Tin Halide Perovskite Nanocrystals. *J. Am. Chem. Soc.* **2016**, *138*, 2941−2944.
(46) Leng, M.; Chen, Z.; Yang, Y.; Li, Z.; Zeng, K.; Li, K.; Niu, G.; He, Y.; Zhou, Q.; Tang, J. Lead-Free, Blue Emitting Bismuth Halide Perovskite Quantum Dots. *Angew. Chem., Int. Ed.* **2016**, *55*, 15012−15016.
(47) Swarnkar, A.; Marshall, A. R.; Sanehira, E. M.; Chernomordik, B. D.; Moore, D. T.; Christians, J. A.; Chakrabarti, T.; Luther, J. M. Quantum Dot-Induced Phase Stabilization of α-$CsPbI_3$ Perovskite for High-Efficiency Photovoltaics. *Science* **2016**, *354*, 92−95.
(48) Fang, Y.; Dong, Q.; Shao, Y.; Yuan, Y.; Huang, J. Highly Narrowband Perovskite Single-Crystal Photodetectors Enabled by Surface-Charge Recombination. *Nat. Photonics* **2015**, *9*, 679−686.
(49) Dong, Q.; Fang, Y.; Shao, Y.; Mulligan, P.; Qiu, J.; Cao, L.; Huang, J. Electron-Hole Diffusion Lengths > 175 μm in Solution-Grown $CH_3NH_3PbI_3$ Single Crystals. *Science* **2015**, *347*, 967−970.
(50) Park, B.-W.; Philippe, B.; Zhang, X.; Rensmo, H.; Boschloo, G.; Johansson, E. M. J. Bismuth Based Hybrid Perovskites $A_3Bi_2I_9$ (A: Methylammonium or Cesium) for Solar Cell Application. *Adv. Mater.* **2015**, *27*, 6806−6813.
(51) Liu, W.; Lin, Q.; Li, H.; Wu, K.; Robel, I.; Pietryga, J. M.; Klimov, V. I. Mn^{2+}-Doped Lead Halide Perovskite Nanocrystals with Dual-Color Emission Controlled by Halide Content. *J. Am. Chem. Soc.* **2016**, *138*, 14954−14961.

DOI: 10.1021/acsnano.6b08747
ACS Nano 2017, 11, 2239−2247

(52) Parobek, D.; Roman, B. J.; Dong, Y.; Jin, H.; Lee, E.; Sheldon, M.; Son, D. H. Exciton-to-Dopant Energy Transfer in Mn-Doped Cesium Lead Halide Perovskite Nanocrystals. *Nano Lett.* **2016**, *16*, 7376−7380.
(53) Vlaskin, V. A.; Janssen, N.; van Rijssel, J.; Beaulac, R.; Gamelin, D. R. Tunable Dual Emission in Doped Semiconductor Nanocrystals. *Nano Lett.* **2010**, *10*, 3670−3674.
(54) Xie, R.; Peng, X. Synthesis of Cu-Doped InP Nanocrystals (d-dots) with ZnSe Diffusion Barrier as Efficient and Color-Tunable NIR Emitters. *J. Am. Chem. Soc.* **2009**, *131*, 10645−10651.
(55) Vlaskin, V. A.; Barrows, C. J.; Erickson, C. S.; Gamelin, D. R. Nanocrystal Diffusion Doping. *J. Am. Chem. Soc.* **2013**, *135*, 14380−14389.
(56) Magana, D.; Perera, S. C.; Harter, A. G.; Dalal, N. S.; Strouse, G. F. Switching-On Superparamagnetism in Mn/CdSe Quantum Dots. *J. Am. Chem. Soc.* **2006**, *128*, 2931−2939.
(57) Stowell, C. A.; Wiacek, R. J.; Saunders, A. E.; Korgel, B. A. Synthesis and Characterization of Dilute Magnetic Semiconductor Manganese-Doped Indium Arsenide Nanocrystals. *Nano Lett.* **2003**, *3*, 1441−1447.
(58) Norris, D. J. High-Quality Manganese-Doped ZnSe Nanocrystals. *Nano Lett.* **2001**, *1*, 3−7.
(59) Lv, L.; Xu, Y.; Fang, H.; Luo, W.; Xu, F.; Liu, L.; Wang, B.; Zhang, X.; Yang, D.; Hu, W.; Dong, A. Generalized Colloidal Synthesis of High-Quality, Two-Dimensional Cesium Lead Halide Perovskite Nanosheets and Their Applications in Photodetectors. *Nanoscale* **2016**, *8*, 13589−13596.
(60) Mahamuni, S.; Lad, A. D.; Patole, S. Photoluminescence Properties of Manganese-Doped Zinc Selenide Quantum Dots. *J. Phys. Chem. C* **2008**, *112*, 2271−2277.
(61) Koolyk, M.; Amgar, D.; Aharon, S.; Etgar, L. Kinetics of Cesium Lead Halide Perovskite Nanoparticle Growth; Focusing and De-Focusing of Size Distribution. *Nanoscale* **2016**, *8*, 6403−6409.
(62) Zhou, D.; Liu, M.; Lin, M.; Bu, X.; Luo, X.; Zhang, H.; Yang, B. Hydrazine-Mediated Construction of Nanocrystal Self-Assembly Materials. *ACS Nano* **2014**, *8*, 10569−10581.

DOI: 10.1021/acsnano.6b08747
ACS Nano 2017, 11, 2239−2247